ARTICLES

Two-photon excitation spectroscopy of $4f^7 \rightarrow 4f^7$ transitions of Eu^{2+} ions doped in a $KMgF_3$ crystal

H. J. Seo,[1,*] B. K. Moon,[1] and T. Tsuboi[2]
[1]*Department of Physics, Pukyong National University, Daeyeon 3-Dong, Namgu, Pusan 608-737, Republic of Korea*
[2]*Faculty of Engineering, Kyoto Sangyo University, Kamigamo, Kita-ku, Kyoto 603-8555, Japan*
(Received 29 March 2000; revised manuscript received 5 July 2000)

Intraconfiguration $4f^7 \rightarrow 4f^7$ transitions of Eu^{2+} in $KMgF_3$ have been investigated by two-photon excitation (TPE) spectroscopy at 10 K. Emission bands due to the $^6P_{7/2} \rightarrow {}^8S_{7/2}$ and $^6I_{7/2} \rightarrow {}^8S_{7/2}$ transitions are obtained by two-photon excitation into the ^6I_J (J=7/2,9/2,17/2,11/2,15/2,13/2) and ^6D_J (J=1/2,7/2,3/2,5/2) states. The TPE spectrum of the $^6I_{7/2} \rightarrow {}^8S_{7/2}$ emission is observed to be different from that of the $^6P_{7/2} \rightarrow {}^8S_{7/2}$ emission. This is explained by the relative positions of the lowest crystal-field component of the $^6I_{7/2}$ level and the lowest level of the $4f^6 5d$ configuration for cubic-site and non-cubic-site Eu^{2+} ions. The observed TPE spectra are satisfactorily interpreted by a suggestion that the $^6I_{7/2} \rightarrow {}^8S_{7/2}$ emission is produced by only cubic-site Eu^{2+}, while the $^6P_{7/2} \rightarrow {}^8S_{7/2}$ emission is produced by both cubic-site Eu^{2+} and non-cubic-site Eu^{2+}.

I. INTRODUCTION

The divalent europium ion Eu^{2+} has the $4f^7 5s^2 5p^6$ (named $4f^7$ hereafter) electronic configuration as the ground state and $4f^6 5s^2 5p^6 5d (4f^6 5d)$ as the first excited electronic configuration. The interconfigurational electronic $4f^7(^8S_{7/2}) \rightarrow 4f^6 5d$ transition is parity allowed, while the intraconfigurational $4f^7 \rightarrow 4f^7$ transition is parity-forbidden and the electric dipole transition is not allowed. Therefore the optical absorption bands due to the latter transition are much weaker than the absorption bands due to the former transition. Additionally the $4f^7 \rightarrow 4f^7$ absorption bands appear close to the very intense bands due to the parity-allowed transition.[1–3] For that reason it is difficult to clarify the high-lying excited states of the $4f^7$ configuration in one-photon spectroscopy. Two-photon excitation (TPE) spectroscopy, however, is useful to investigate high-lying levels of the $4f^7$ configuration, which are located close to the levels of the $4f^6 5d$ configuration, because the electric-dipole-forbidden $4f^7 \rightarrow 4f^7$ transition becomes parity allowed for two-photon transitions.

The $4f^7$-$4f^7$ transitions of Eu^{2+} have been intensively studied in fluoride crystals,[3–7] where narrow excitation lines of the $4f^7$ levels are observed in TPE spectra. The $4f^7$ levels of Eu^{2+} in $KMgF_3$ have been investigated by absorption,[3] emission,[4,5] one-photon excitation[5] (OPE), and TPE (Refs. 6,7) spectroscopy. Ellens *et al.* observed two kinds of emission band by OPE with 308 nm radiation.[5] One is a band at around 359 nm; the other is a band with peak at about 322 nm. The 322 nm emission is observed below 20 K, while the 359 nm emission is observed even at room temperature. The 322 nm emission has been attributed to the $^6I_{7/2} \rightarrow {}^8S_{7/2}$ transition and the 359 nm emission to the $^6P_{7/2} \rightarrow {}^8S_{7/2}$ transition. The 322 nm emission is called the $^6I_{7/2}$ emission hereafter, while the 359 nm emission is called the $^6P_{7/2}$ emission. By OPE of Eu^{2+} in $KMgF_3$, it was found that the lowest level of the $4f^6 d$ configuration is situated just above the lowest crystal-field component of the $^6I_{7/2}$ level.[5]

The TPE spectra of Eu^{2+} in $KMgF_3$ were studied by Francini *et al.* by monitoring the $^6P_{7/2}$ emission.[6,7] The $4f^7$ configuration has the excited states ^6P_J ($J=\frac{7}{2},\frac{5}{2},\frac{3}{2}$), ^6I_J ($J=\frac{7}{2},\frac{9}{2},\frac{17}{2},\frac{11}{2},\frac{15}{2},\frac{13}{2}$) and ^6D_J ($J=\frac{9}{2},\frac{1}{2},\frac{7}{2},\frac{3}{2},\frac{5}{2}$). To our knowledge, no study of two-photon spectroscopy has been undertaken for the $4f^7$ excited states except for the $^6P_{7/2}$, $^6P_{5/2}$, and $^6D_{9/2}$ states studied by Francini *et al.*[6,7] Moreover we know of no study of TPE by monitoring the $^6I_{7/2}$ emission. In the present paper, we investigate two-photon-excited transitions from the $^8S_{7/2}$ ground state to the $4f^7$ excited states by monitoring not only the $^6P_{7/2}$ emission but also the $^6I_{7/2}$ emission to clarify the $4f^7$ levels of Eu^{2+} in $KMgF_3$.

By analogy with the case of isoelectronic Gd^{3+},[8–12] the $4f^7$ configuration of Eu^{2+} has the excited states $^6P_{7/2}$, $^6P_{5/2}$, $^6P_{3/2}$, $^6I_{7/2}$, $^6I_{9/2}$, $^6I_{17/2}$, $^6I_{11/2}$, $^6I_{15/2}$, $^6I_{13/2}$, $^6D_{9/2}$, $^6D_{1/2}$, $^6D_{7/2}$, $^6D_{3/2}$, and $^6D_{5/2}$ in order of increasing energy. However, the order has not been established for the $^6I_{17/2}$, $^6I_{11/2}$, $^6I_{15/2}$, and $^6I_{13/2}$ levels of Eu^{2+} yet, as seen in the cases of Eu^{2+} in CaF_2, SrF_2, KBr, and NaCl.[13,14] Here we try to determine the order of energy levels of Eu^{2+} from the TPE spectroscopy of $KMgF_3$.

In $KMgF_3$, the K^+ ion with ionic radius of 1.78 Å is coordinated by a cubic twelvefold F^- ion and surrounded by Mg^{2+} ions with smaller radius (0.86 Å).[15] The Eu^{2+} ion (1.49 Å) substitutes for the singly charged K^+ ion. This gives rise to formation of a charge compensating positive ion vacancy located at one of the K^+ sites. If such a vacancy is located close to Eu^{2+}, this leads to the presence of Eu^{2+} at noncubic sites, i.e., Eu^{2+} with tetragonal (C_{4v}) and trigonal (e.g., C_{3v}) site symmetries.[3] If the vacancy is located far from Eu^{2+}, one can assume that such an Eu^{2+} ion has cubic site symmetry. The energies of the cubic- and non-cubic-site Eu^{2+} ions have been clarified for the $^6P_{7/2}$, $^6P_{5/2}$, and $^6D_{9/2}$ manifolds,[6,7] but not for the other manifolds. Here we also investigate the ^6D_J ($J=\frac{1}{2},\frac{7}{2},\frac{3}{2},\frac{5}{2}$) and ^6I_J ($J=\frac{7}{2},\frac{9}{2},\frac{17}{2},\frac{11}{2},\frac{15}{2},\frac{13}{2}$) states by two-photon spectroscopy to

confirm the presence of the cubic- and non-cubic-site Eu^{2+} ions and to clarify the location of their energy states relative to the $4f^6 5d$ level which is located close to the ^6D_J and ^6I_J levels.

II. EXPERIMENTAL PROCEDURE

A single crystal of $KMgF_3$ doped with Eu^{2+} ions (0.5 mol %) was grown from the melt in Ar-gas atmosphere by the Czochralski method at Pukyong National University. The starting material was prepared by mixing KF and MgF_2 in a molar ratio of 1:1, and then was annealed for 1 h at 150 °C and heated up to the melting temperature in a furnace filled with Ar gas with a chamber pressure of 1.5 atm. The pulling speed was 5 mm/h and the rotation was 10 rpm. Single crystals up to 5 cm in length and 2 cm in diameter were successfully pulled. The crystal was cut and polished along the crystal axis to a size of $3\times5\times6$ mm^3.

The excitation source was a dye laser (Spectron Laser Sys. SL4000) pumped by the second harmonic (532 nm) of a pulsed Nd:YAG (yttrium aluminum garnet) laser (Spectron Laser Sys. SL802G). The dyes used were R590, R590 + 610, and DCM, which have scanning ranges of 557–572, 574–590, and 610–660 nm, respectively. The wavelength of the dye laser output was read by a wavelength meter (New Focus Inc. 7711) with a wavelength accuracy of 0.01 nm. The repetition rate of the dye laser output was 10 Hz with 5 ns duration. The typical linewidth of the dye laser output was about 0.03 cm^{-1} at 580 nm. The laser beam was focused inside the sample with a cross-sectional area of about 3 mm^2. The pulse energy was varied up to 15 mJ, which gives a peak power of 100 MW/cm^2 at the irradiated area. The excitation was performed with a laser beam linearly polarized parallel to the [010] axis and propagating along the [001] direction of the crystal. The sample was cooled in a liquid helium flow cryostat and measurements were performed at 10 K. The fluorescence from the crystal following the excitation was collected in the direction of the [100] axis perpendicular to the incident laser beam. Suitable filters were used to eliminate noise due to the scattered laser radiation. The TPE spectra were recorded by monitoring the fluorescence at 322 and 359 nm. The fluorescence was dispersed by a 75 cm monochromator (Acton Research Corp. Pro-750) and observed with a photomultiplier tube (PMT) (Hamamatsu R928). The slit width of the monochromator was set to a spectral resolution of about 60 cm^{-1} for the measurements of the TPE spectra. The signal from the PMT was fed into a digital oscilloscope (LeCroy 9310) and then the data were stored in a personal computer.

III. EXPERIMENTAL RESULTS

Figure 1(a) shows the two-photon excitation spectrum that was obtained by the excitation with 581.48 nm radiation. Two emission bands are observed at 359 and 322 nm. These emissions agree with those obtained by OPE with 308 nm radiation:[5] the 359 and 322 nm emissions are the $^6P_{7/2}$ and $^6I_{7/2}$ emissions, respectively. The 322 nm emission is much weaker in intensity than the 359 nm emission: the intensity of the former emission is about 1/68 that of the latter. The spectrum was obtained under low spectral resolution of 60 cm^{-1}. When we measured the emission spectrum under higher resolution of 1 cm^{-1}, the 359 nm emission was estimated to have a bandwidth of 14 cm^{-1} [see Fig. 1(b)], while the 322 nm emission was too weak to estimate the bandwidth precisely. As shown in Fig. 1(b), the 359 nm emission band is observed to consist of at least four components and vibronic structure is observed at the low-energy side (in the region of 360–368 nm). Not only the splitting of the main 359 nm emission band but also the vibronic structure are consistent with those observed by Ellens *et al.* at 4.2 K,[5] although their spectrum is better resolved than our spectrum, which was measured at 10 K. The $^6D_{9/2}$ state is located at 34 380–34 400 cm^{-1} above the $^8S_{7/2}$ ground state[6,7] which means that the 581.48 nm radiation (the corresponding photon energy is 17 197 cm^{-1}) excites the Eu^{2+} ions into the $^6D_{9/2}$ level by a two-photon process. It is concluded that the observed 322 and 359 nm two-photon excited emissions are produced after a nonradiative decay process to the $^6I_{7/2}$ and $^6P_{7/2}$ levels, respectively, from the upper $^6D_{9/2}$ level.

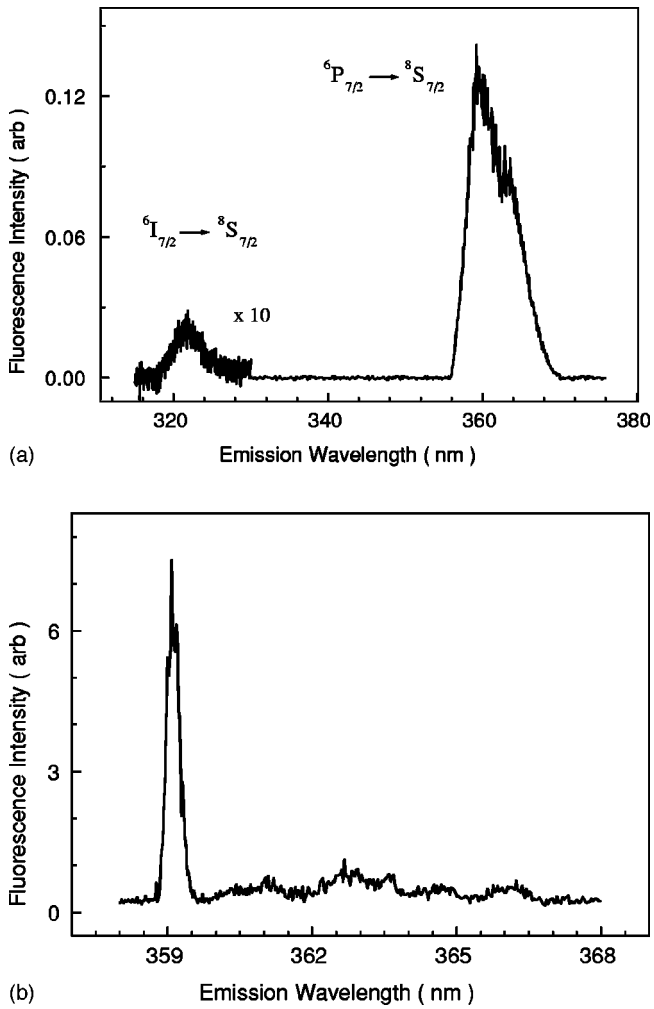

FIG. 1. Two-photon excited emission spectra of Eu^{2+} in $KMgF_3$ crystal obtained by excitation with 581.48 nm radiation at 10 K. (a) Low-resolution (60 cm^{-1}) spectrum in the $^6P_{7/2}\rightarrow{}^8S_{7/2}$ and $^6I_{7/2}\rightarrow{}^8S_{7/2}$ regions. (b) High-resolution (1 cm^{-1}) spectrum in the $^6P_{7/2}\rightarrow{}^8S_{7/2}$ region, in which vibronic structure is observed in the spectral range of 360–368 nm.

Figure 2 shows the TPE spectra in the spectral range of the $^8S_{7/2}\rightarrow{}^6D_{9/2}$ transition obtained by monitoring the 322

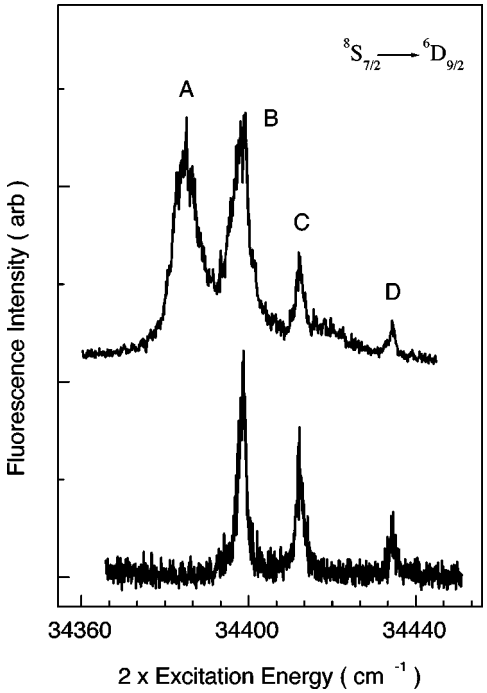

FIG. 2. TPE spectra in the spectral range of the $^8S_{7/2} \rightarrow {}^6D_{9/2}$ transition for the $^6I_{7/2}$ emission (shown in the lower part of the figure) and the $^6P_{7/2}$ emission (upper part) at 10 K.

and 359 nm emissions. We note that the TPE spectrum for the $^6I_{7/2}$ emission (lower part of Fig. 2) is different from that for the $^6P_{7/2}$ emission (upper part of Fig. 2). The latter consists of four lines at 34 384, 34 399, 34 412, and 34 434 cm^{-1} (named *A*, *B*, *C*, and *D*, respectively, as indicated in the figure). The TPE spectrum for the $^6I_{7/2}$ emission consists of the same *B*, *C*, and *D* lines but not the *A* line. The lines of the TPE spectrum for the $^6P_{7/2}$ emission are broader than those for the $^6I_{7/2}$ emission. The TPE spectrum for the 359 nm emission (i.e., $^6P_{7/2}$ emission) is similar to the spectrum obtained by Francini *et al.* using a laser beam linearly polarized parallel to the [010] crystal axis, which is the same as our laser beam.[6] However, there is a difference between Francini *et al.*'s spectra and ours. The intensity of the 34 384 cm^{-1} line (*A* line) is almost the same as that of the 34 399 cm^{-1} line (*B* line) in our spectrum, while the former is about $\frac{1}{4}$ of the latter in Francini *et al.*'s spectrum.

The lifetimes of the $^6P_{7/2}$ and $^6I_{7/2}$ emissions were measured at different excitation lines at 10 K. The temporal evolution of all the fluorescence exhibits a single-exponential decay curve. The lifetimes of the $^6I_{7/2}$ emission by the excitation at the *B*, *C*, and *D* lines were estimated to be 37 μs, which is consistent with the result of one-photon excitation by Ellens *et al.* (see Fig. 8 of Ref. 5). For the $^6P_{7/2}$ emission, the lifetimes were obtained as 6.9 ms and 5.2 ms by excitations at the *B*, *C*, and *D* lines and by the excitation at the *A* line, respectively.

Figure 3 shows the TPE spectra in the spectral range of the $^8S_{7/2} \rightarrow {}^6D_J$ ($J = \frac{1}{2}, \frac{7}{2}, \frac{3}{2}, \frac{5}{2}$) transitions obtained by monitoring the 322 and 359 nm emissions. The enlarged TPE spectrum in the spectral range of the $^8S_{7/2} \rightarrow {}^6D_{7/2}$ transition is shown in Fig. 4. The TPE lines corresponding to the $^8S_{7/2} \rightarrow {}^6D_{1/2}$, $^6D_{7/2}$, $^6D_{3/2}$, and $^6D_{5/2}$ transitions are observed at around 34 990, 35 100–35 190, 35 200–35 250, and

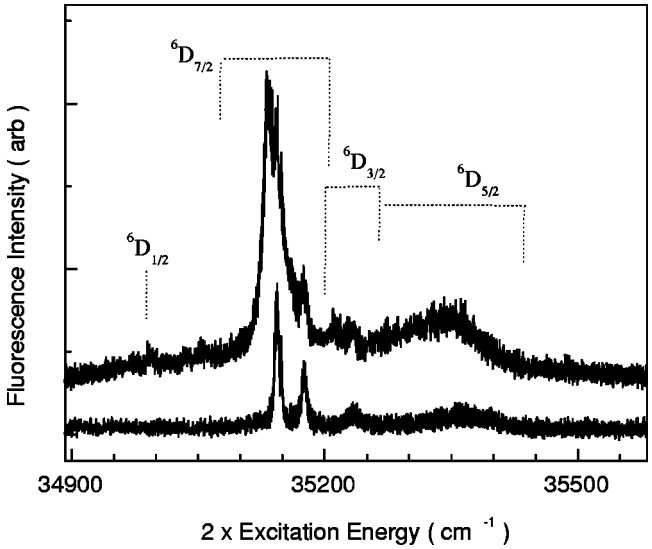

FIG. 3. TPE spectra in the spectral range of the $^8S_{7/2} \rightarrow {}^6D_J$ ($J = \frac{1}{2}, \frac{7}{2}, \frac{3}{2}, \frac{5}{2}$) transitions for the $^6I_{7/2}$ emission (shown in the lower part of the figure) and $^6P_{7/2}$ emission (upper part) at 10 K. The transitions from the $^8S_{7/2}$ state to the different ^6D_J levels are indicated.

35 300–35 450 cm^{-1}. These line positions are about 500 cm^{-1} above the corresponding Eu^{2+} lines that are observed in CaF_2.[13] The observed levels thus are attributable to the excited levels of the $4f^7$ configuration as indicated in Fig. 3. It is noted that the line due to the $^8S_{7/2} \rightarrow {}^6D_{7/2}$ transition is much more intense than the other lines. Figure 5 shows the TPE spectra in the spectral range of the $^8S_{7/2} \rightarrow {}^6I_J$ ($J = \frac{7}{2}, \frac{9}{2}, \frac{17}{2}, \frac{11}{2}, \frac{15}{2}, \frac{13}{2}$) transitions obtained by monitoring the 322 and 359 nm emissions. The enlarged TPE spectra in the spectral range of the $^8S_{7/2} \rightarrow {}^6I_{7/2}$, $^8S_{7/2} \rightarrow {}^6I_{9/2}$, $^8S_{7/2} \rightarrow {}^6I_{17/2}$, $^8S_{7/2} \rightarrow {}^6I_{11/2}$, and $^8S_{7/2} \rightarrow {}^6I_{15/2,13/2}$ transitions are shown in Figs. 6, 7, 8, 9, and 10, respectively. The TPE lines corresponding to the $^8S_{7/2} \rightarrow {}^6I_{7/2}$, $^8S_{7/2} \rightarrow {}^6I_{9/2}$, $^8S_{7/2} \rightarrow {}^6I_{17/2}$, $^8S_{7/2} \rightarrow {}^6I_{11/2}$, and $^8S_{7/2} \rightarrow {}^6I_{15/2,13/2}$ transitions are observed at 31 250–31 360, 31 560–31 620, 31 690–31 770,

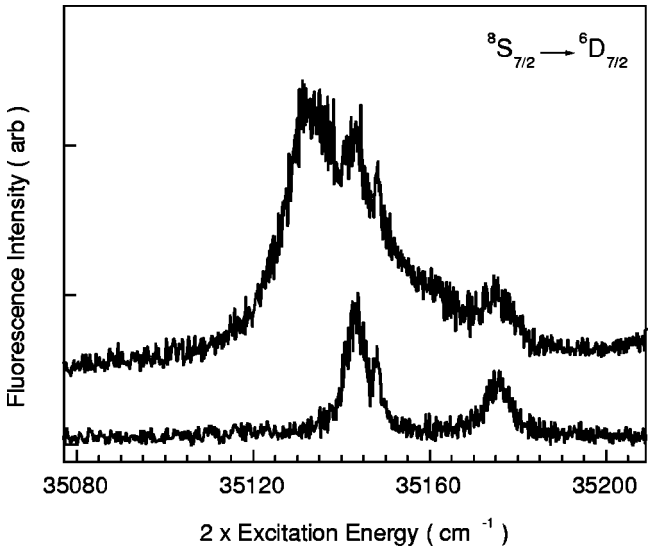

FIG. 4. Enlarged TPE spectra of Fig. 3 in the spectral range of the $^8S_{7/2} \rightarrow {}^6D_{7/2}$ transition.

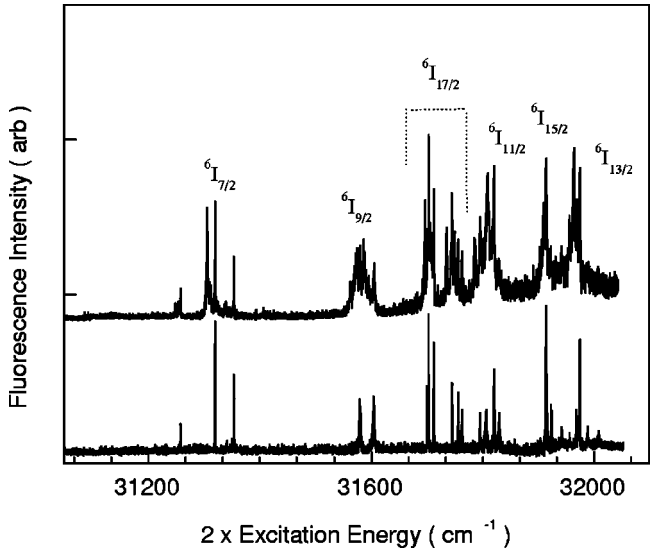

FIG. 5. TPE spectra in the spectral range of the $^8S_{7/2}\rightarrow{}^6I_J$ ($J=\frac{7}{2},\frac{9}{2},\frac{17}{2},\frac{11}{2},\frac{15}{2},\frac{13}{2}$) transitions for the $^6I_{7/2}$ emission (shown in the lower part of the figure) and the $^6P_{7/2}$ emission (upper part) at 10 K. The transitions from the $^8S_{7/2}$ state to the different ^6I_J levels are indicated.

31 780–31 840, and 31 900–32 020 cm^{-1}, respectively. Like the $^8S_{7/2}\rightarrow{}^6D_J$ transitions, these line positions are about 500 cm^{-1} above the corresponding Eu^{2+} lines in CaF_2.[13]

We note that the linewidths observed in the TPE spectrum in the range of the $^8S_{7/2}\rightarrow{}^6I_J$ transitions are considerably narrower than the TPE lines in the $^8S_{7/2}\rightarrow{}^6D_J$ region. In all the spectral ranges of the $^8S_{7/2}\rightarrow{}^6I_J$ and ^6D_J transitions the number of lines observed in the TPE spectrum for the $^6I_{7/2}$ emission is smaller than that for the $^6P_{7/2}$ emission. Ellens *et al.* observed lines at 31 269, 31 287, 31 307, and 31 320 cm^{-1} and several weak lines below 31 250 cm^{-1} in the OPE spectrum for the $^6P_{7/2}$ emission in the $^8S_{7/2}\rightarrow{}^6I_{7/2}$ transition region at 4.2 K.[5] Lines corresponding to the 31 269, 31 307, and 31 320 cm^{-1} lines are observed in the present TPE spectra, but the other lines are not observed, as shown in Fig. 6.

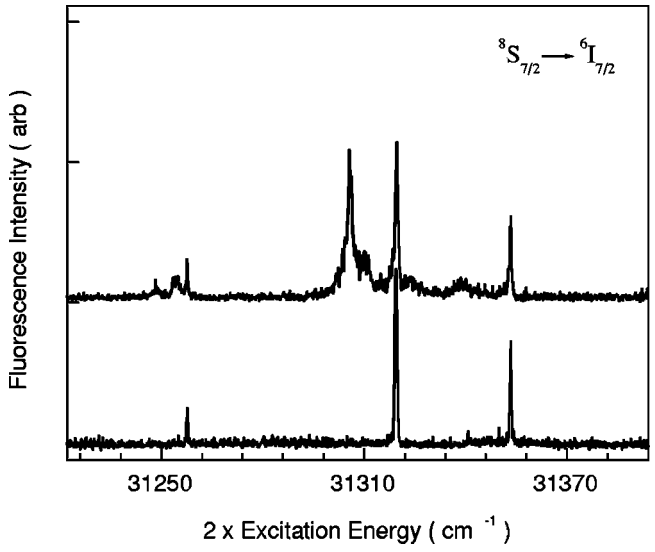

FIG. 6. Enlarged TPE spectra of Fig. 5 in the spectral range of the $^8S_{7/2}\rightarrow{}^6I_{7/2}$ transition.

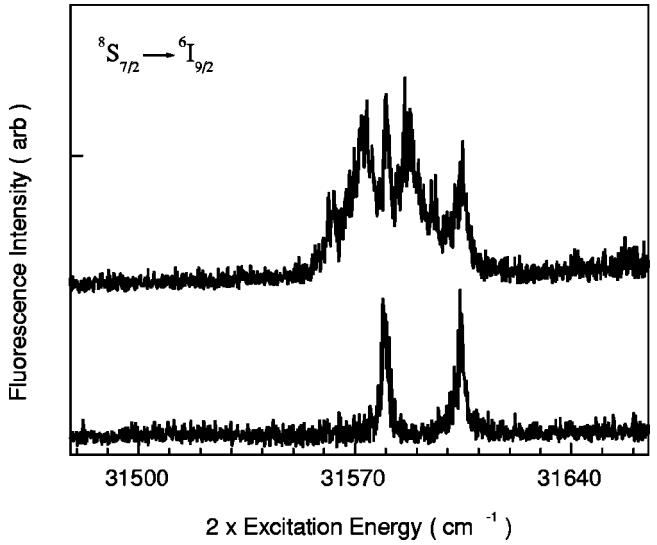

FIG. 7. Enlarged TPE spectra of Fig. 5 in the spectral range of the $^8S_{7/2}\rightarrow{}^6I_{9/2}$ transition.

IV. DISCUSSION

The 322 nm emission is observed to be much weaker than the 359 nm emission. As one of the reasons for the relatively weak intensity of the $^6I_{7/2}$ emission, nonradiative transition is conceivable. The energy gap between the $^6I_{7/2}$ level and the $^6P_{3/2}$ level (which is at 28 670 cm^{-1})[4] is about 2600 cm^{-1}. Thus the gap can be bridged by five phonons because the highest phonon energy of $KMgF_3$ is 530 cm^{-1},[4] indicating that the nonradiative multiphonon decay rate from the $^6I_{7/2}$ level could be comparable with the radiative decay rate from the $^6I_{7/2}$ level to the $^8S_{7/2}$ level. According to Sytsma *et al.*, the intensity ratio of the $^6I_{7/2}$ emission to the $^6P_{7/2}$ emission is given by W_r/W_{nr}, where W_r and W_{nr} are the radiative and nonradiative decay probabilities from the $^6I_{7/2}$ level, respectively.[16] In the case of Gd^{3+} in YOCl, where $W_r=398$ s^{-1} and $W_{nr}=4730$ s^{-1},[16] the intensity ratio is estimated to be 1/11.9. This value is quite different from our

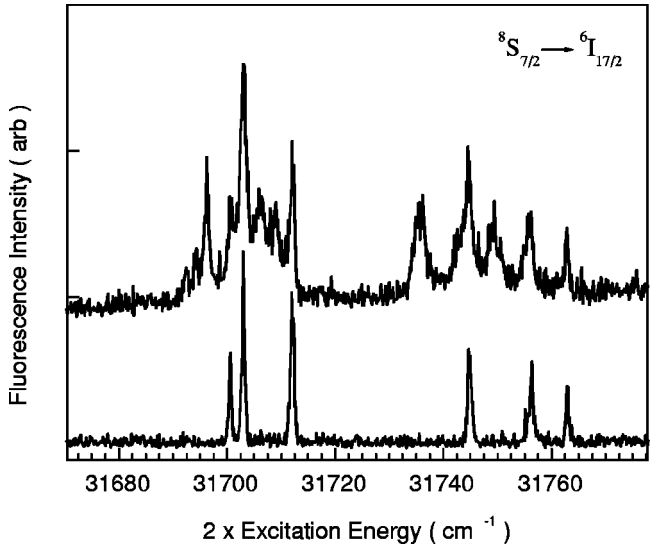

FIG. 8. Enlarged TPE spectra of Fig. 5 in the spectral range of the $^8S_{7/2}\rightarrow{}^6I_{17/2}$ transition.

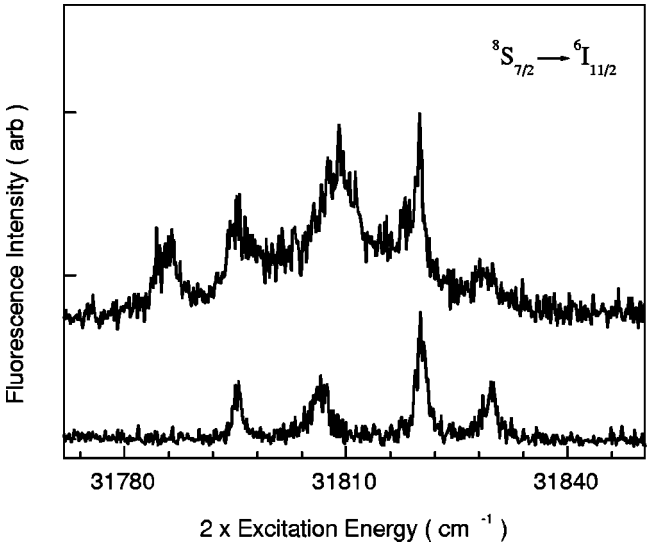

FIG. 9. Enlarged TPE spectra of Fig. 5 in the spectral range of the $^8S_{7/2} \rightarrow {}^6I_{11/2}$ transition.

ratio of 1/68 although the $^6I_{7/2}$ emission is much weaker than the $^6P_{7/2}$ emission in both samples. It is suggested that the nonradiative decay probability W_{nr} is much higher for Eu^{2+} in $KMgF_3$ than for Gd^{3+} in YOCl. Therefore it is understandable that the 322 nm $^6I_{7/2}$ emission is much weaker than the 359 nm $^6P_{7/2}$ emission. Another reason for the difference of the ratio is that the $^6P_{7/2}$ emission is caused by both cubic- and non-cubic-site Eu^{2+} but the $^6I_{7/2}$ emission is caused by only cubic-site Eu^{2+} as mentioned below.

Ellens *et al.* reported the lifetimes of 7.3, 5.8, and 6.7 ms for the $^6P_{7/2}$ emission at 27 836.9, 27 833.1, and 27 820.3 cm^{-1}, respectively, obtained by high-resolution emission spectroscopy at 4.2 K under OPE with 308 nm radiation.[5] They assigned the 27 836.9 cm^{-1} emission to Eu^{2+} at the cubic site in view of the longest lifetime of 7.3 ms and the smallest linewidth. It is suggested that the values of 6.9 ms obtained for the *B*, *C*, and *D* lines and 5.2 ms obtained for the *A* line in the TPE spectrum for the $^6P_{7/2}$ emission correspond to the values of 7.3 and 5.8 ms reported by Ellens *et al.* The lifetimes obtained by us are shorter than those of Ellens *et al.* This difference is due to the difference of the crystal temperature. We measured at 10 K, while Ellens *et al.* measured at 4.2 K. It is conceivable that the *B*, *C*, and *D* lines are due to Eu^{2+} at the cubic site, while the *A* line is due to Eu^{2+} at the noncubic site. This is consistent with the assignment by Francini *et al.*[6,7] The $^6P_{7/2}$ emission spectrum was observed to consist of at least four components [see Fig. 1(b)]. The appearance of such components is caused by the presence of Eu^{2+} ions with different site symmetries.[5] Accordingly, the presence of cubic- and non-cubic-site Eu^{2+} ions is confirmed from not only the TPE spectrum but also the emission spectrum.

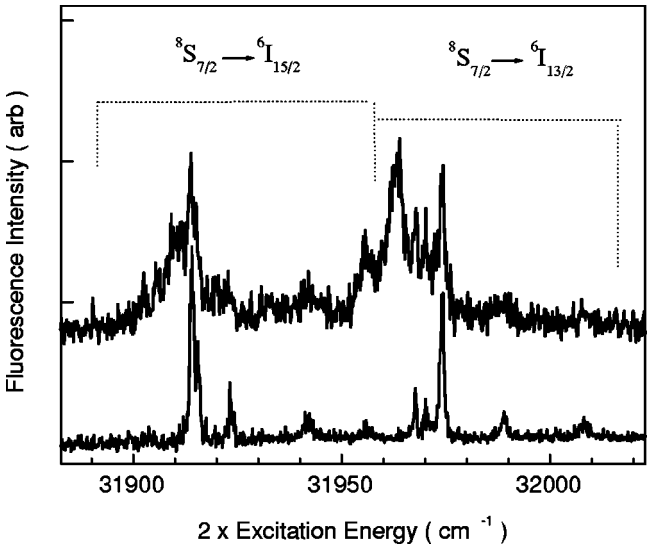

FIG. 10. Enlarged TPE spectra of Fig. 5 in the spectral range of the $^8S_{7/2} \rightarrow {}^6I_{15/2,13/2}$ transitions.

The *B*, *C*, and *D* lines due to cubic-site Eu^{2+} are observed in the TPE spectrum for the $^6I_{7/2}$ emission, but the *A* line due to non-cubic-site Eu^{2+} is not observed. The *A* line is observed in the TPE spectrum only for the $^6P_{7/2}$ emission. This is explained as follows. According to the results of OPE spectroscopy by Ellens *et al.*,[5] the $^6I_{7/2}$ level is located about 50 cm^{-1} below the lowest $4f^6 5d$ level for cubic-site Eu^{2+} in $KMgF_3$. According to Francini *et al.*, the $^6P_{7/2}$ and $^6P_{5/2}$ levels of non-cubic-site Eu^{2+} with trigonal symmetry are shifted slightly toward lower energy compared to those of cubic-site Eu^{2+}.[6] Such a low-energy shift is also expected for the $^6I_{7/2}$ level of non-cubic-site Eu^{2+}. On the other hand, a larger low-energy shift is expected for the lowest $4f^6 5d$ level than for the $^6I_{7/2}$ level because the $5d$ electron is much more strongly influenced by the crystal field than the $4f$ electron of the inner shell, which enhances the splitting of the $5d$ level with increasing crystal field. For that reason we suggest that, unlike the case of cubic-site Eu^{2+}, the $^6I_{7/2}$ level is above the lowest $4f^6 5d$ level for non-cubic-site Eu^{2+}, as shown in Fig. 11.

The broad *A* TPE line due to non-cubic-site Eu^{2+} is observed at the low-energy side of the narrow *B* line due to cubic-site Eu^{2+} in the $^8S_{7/2} \rightarrow {}^6D_{9/2}$ region (see Fig. 2). That is to say, one broad band due to non-cubic-site Eu^{2+} appears at the low-energy side of the lowest-energy line due to cubic-site Eu^{2+}. It is noted that such a phenomenon is observed not only in the $^8S_{7/2} \rightarrow {}^6D_{9/2}$ region but also in all the other regions. For example, in the $^6I_{7/2}$ region (see Fig. 6) a broad line due to non-cubic-site Eu^{2+} appears at 31 248 cm^{-1}, which is on the low-energy side of the lowest-energy cubic-site Eu^{2+} line at 31 258 cm^{-1}. This indicates that the redshift in the $^6P_{7/2}$ and $^6P_{5/2}$ levels of non-cubic-site Eu^{2+}, which has been theoretically derived,[6] is also true for all the ^6D_J and ^6I_J levels.

When non-cubic-site Eu^{2+} ions are excited into the ^6D_J and ^6I_J levels, the excited Eu^{2+} ions rapidly relax to the lowest $^6P_{7/2}$ level of the ^6P_J manifolds through nonradiative relaxation into the lowest-energy $4f^6 5d$ level, and then decay radiatively to the $^8S_{7/2}$ ground level, giving rise to the $^6P_{7/2}$ emission. On the other hand, when cubic-site Eu^{2+} ions are excited into the ^6D_J and ^6I_J levels, they nonradiatively relax to the lowest $4f^6 5d$ level and then to the $^6I_{7/2}$ level, from which some ions relax to the $^8S_{7/2}$ ground level giving rise to the $^6I_{7/2}$ emission, and the other ions nonradiatively relax to the $^6P_{7/2}$ level and then give rise to the $^6P_{7/2}$ emission. Two kinds of emission are thus observed after ex-

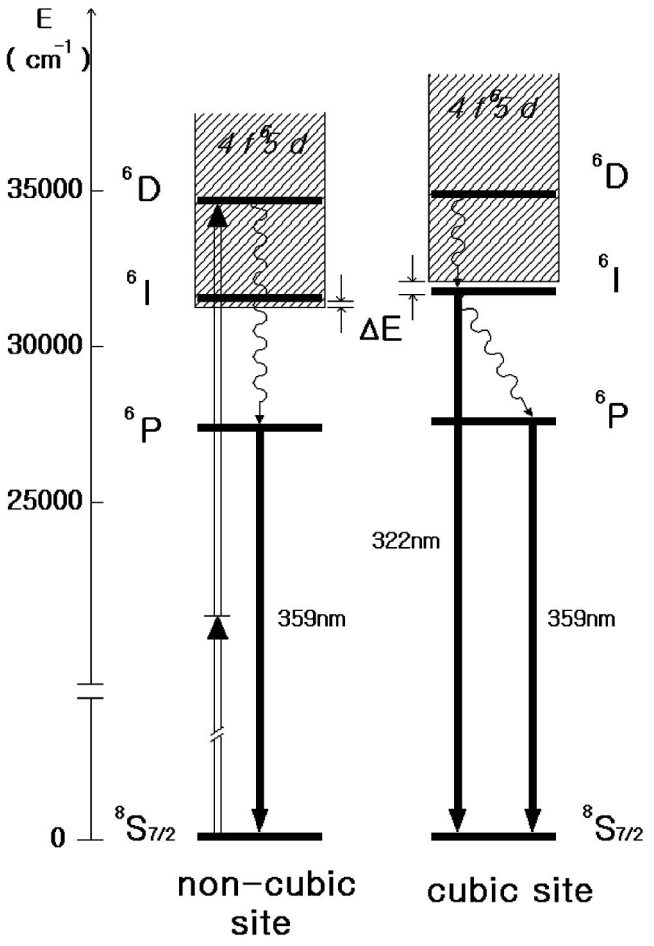

FIG. 11. Energy level diagram of cubic- and non-cubic-site Eu^{2+} in $KMgF_3$. Two-photon excitation, relaxation, and emission are indicated by arrows.

citation into the ^6D_J and ^6I_J manifolds. This suggests that the $^6I_{7/2}$ emission is produced by only cubic-site Eu^{2+}, while the $^6P_{7/2}$ emission is produced by not only cubic-site Eu^{2+} but also non-cubic-site Eu^{2+}.

Of the ^6P_J, ^6I_J, and ^6D_J manifolds, it is unknown whether the $^6I_{15/2}$ level is lower in energy than the $^6I_{13/2}$ level or not, as for Eu^{2+} in CaF_2 and SrF_2.[13] The same is true for isoelectronic Gd^{3+} in $Cs_2NaGdCl_6$.[17,18] The reason is that the crystal-field splittings of these manifolds overlap each other and we are unable to make a definite J assignment. However, considering that the $^6I_{13/2}$ level of Gd^{3+} is observed to be higher than the $^6I_{15/2}$ level in various materials such as $LaCl_3$,[8–11] we assume the same is also true for Eu^{2+} in $KMgF_3$, although Carnall *et al.* have indicated the reverse for $GdCl_3 \cdot 6H_2O$.[19]

Ten sharp lines are observed in the TPE spectrum for the $^6I_{7/2}$ emission in the range of the $^8S_{7/2} \rightarrow {}^6I_{15/2}$ and $^6I_{13/2}$ transitions (see Fig. 10). Of the ten lines, five are at the high-energy side of a broad line at 31 909 cm^{-1} and another five lines are at the high-energy side of another broad line at around 31 936 cm^{-1}; these two broad lines are observed in the TPE spectrum for $^6P_{7/2}$ emission. Therefore, taking into account that both the $^6I_{15/2}$ and $^6I_{13/2}$ states split into five Stark components for Eu^{2+} with cubic crystal-field symmetry, the five low-energy lines at 31 914, 31 915, 31 923, 31 942, and 31 956 cm^{-1} are attributable to the Stark components of the low-lying $^6I_{15/2}$ manifold, while the five high-energy lines at 31 968, 31 970, 31 974, 31 989, and 32 008 cm^{-1} are attributable to the Stark components of the high-lying $^6I_{13/2}$ manifold. The average energy of the $^6I_{15/2}$ manifold is 31 930 cm^{-1}, while that of the $^6I_{13/2}$ manifold is 31 982 cm^{-1}. The difference is 52 cm^{-1}, which is consistent with the case of Gd^{3+} (e.g., 38, 39, and 25 cm^{-1} in $LaCl_3$, $GdCl_3$ and LaF_3, respectively[8–10]) although the difference is a little wider than for Gd^{3+}.

Following these suggestions, we identify the lines of the TPE spectra observed in the spectral ranges of the $^8S_{7/2} \rightarrow {}^6D_J$ $(J=\frac{1}{2},\frac{7}{2},\frac{3}{2},\frac{5}{2})$ and $^8S_{7/2} \rightarrow {}^6I_J$ $(J=\frac{7}{2},\frac{9}{2},\frac{17}{2},\frac{11}{2},\frac{15}{2},\frac{13}{2})$ transitions. In Table I the energies of the Stark components are summarized for each of the ^6D_J $(J=\frac{9}{2},\frac{1}{2},\frac{7}{2},\frac{3}{2},\frac{5}{2})$ and ^6I_J $(J=\frac{7}{2},\frac{9}{2},\frac{17}{2},\frac{11}{2},\frac{15}{2},\frac{13}{2})$ manifolds of cubic- and non-cubic-site Eu^{2+}, which are estimated from Figs. 2–10. In this table the Stark-component energies are also shown for the ^6P_J $(J=\frac{7}{2},\frac{5}{2})$ levels of cubic- and non-cubic-site Eu^{2+}, taken from the results of Francini *et al.*[6] As shown in the table, the number of spectral lines obtained for cubic-site Eu^{2+} agrees with that of the Stark components determined from group theoretical analysis for each manifold except for the $^6D_{1/2}$, $^6D_{5/2}$, and $^6I_{9/2}$ manifolds. For example, six and four Stark components are observed for the $^6I_{17/2}$ and $^6I_{11/2}$ manifolds, respectively, which agree with the theoretically determined energy level splittings for Eu^{2+} with cubic symmetry. Regarding the $^6D_{1/2}$ manifold, the TPE signal is too weak to give the location exactly. Regarding the $^6D_{5/2}$ manifold, only one broad band is observed rather than the expected two bands (see Fig. 3). It is assumed that two bands overlap with each other and form the observed broad band. Regarding the $^6I_{9/2}$ manifold (see Fig. 7), it is not clear at this moment why only two bands are observed, contrary to the expected three bands. Therefore, we confirm that our suggestion (i.e., the $^6I_{7/2}$ emission is produced by only cubic-site Eu^{2+}, while the $^6P_{7/2}$ emission is produced by both cubic-site and non-cubic-site Eu^{2+}) is reasonable although there is one exception regarding the $^6I_{9/2}$ manifold.

The TPE spectra in the range of the $^8S_{7/2} \rightarrow {}^6I_J$ transition have been observed in KBr and NaCl by Casalboni *et al.*[14] and in CaF_2 and SrF_2 by Downer *et al.*[13] These spectra were recorded by monitoring emission from the lowest $4f^6 5d$ level to the $^8S_{7/2}$ ground state because the ^6P_J levels are situated above the lowest $4f^6 5d$ level. The TPE lines observed in alkali halides are very broad, while those observed in alkaline-earth fluorides are relatively narrow but broader than those observed for cubic-site Eu^{2+} in $KMgF_3$. Only cubic-site Eu^{2+} ions are present in alkaline-earth fluorides, while non-cubic-site Eu^{2+} ions are present in alkali halides, since divalent Eu^{2+} occupying a monovalent alkali ion site has a charge-compensating vacancy at the nearest neighbor.[3,14] Accordingly, taking into account that relatively broad TPE lines are also observed for non-cubic-site Eu^{2+} in $KMgF_3$, it is concluded that non-cubic-site Eu^{2+} gives much broader TPE lines than cubic-site Eu^{2+}. In the case of non-cubic-site Eu^{2+}, the symmetry-breaking phonon gives rise to strong mixing of the $4f^7$ levels with the $4f^6 5d$ levels even at low temperature, resulting in relatively broad lines. In Fig. 12 we show the average width of lines observed in each of the ^6I_J and ^6D_J manifolds. The linewidth has a tendency to

TABLE I. Energies of the Stark components of the excited states in the $4f^7$ configuration for the cubic- and non-cubic-site Eu^{2+} ions obtained from the TPE spectra, and number n of the Stark components expected from group theory.

Manifold	n	Peak position (cm^{-1}) Cubic-site Eu^{2+}	Non-cubic-site Eu^{2+}
$^6P_{7/2}$	3	27840.3 [a], 27845.8 [a], 27847.3 [a]	27826.0 [a], 27834.0 [a], 27835.0 [a] 27836.8 [a], 27841.5 [a], 27843.7 [a] 27849.8 [a]
$^6P_{5/2}$	2	28267.0 [a], 28270.5 [a]	28261.0 [a], 28262.3 [a], 28269.7 [a] 28271.3 [a]
$^6P_{3/2}$	1	28670 [b]	
$^6I_{7/2}$	3	31257.6, 31319.5, 31353.4	31248.2, 31254.2, 31305.5 31310.3, 31323.3, 31338.9
$^6I_{9/2}$	3	31579.4, 31604.1	31562.2, 31572.6, 31587.3 31595.4
$^6I_{17/2}$	6	31700.6, 31702.9, 31711.9 31744.8, 31756.3, 31762.8	31692.4, 31694.1, 31696.4 31706.2, 31708.9, 31734.8 31749.0
$^6I_{11/2}$	4	31795.3, 31806.8, 31820.2 31829.7	31785.8, 31809.8
$^6I_{15/2}$	5	31914.1, 31915.2, 31923.3 31941.9, 31955.7	31902.5, 31905.4, 31909.3 31911.6, 31917.7, 31919.7 31931.7
$^6I_{13/2}$	5	31967.7, 31970.2, 3197.2 31989.0, 32008.1	31960.1, 31963.2, 31965.5 31972.3
$^6D_{9/2}$	3	34398.7, 34412.1, 34434.4	34385.1, 34418.8
$^6D_{1/2}$	1		34992.1
$^6D_{7/2}$	3	35143.3, 35148.0, 35175.7	35130.1, 35161.4
$^6D_{3/2}$	1	35235.1	35211.7
$^6D_{5/2}$	2	35366.9	35329.8

[a]Obtained by Francini *et al.* (Ref. 6).
[b]Obtained by Altshuler *et al.* (Ref. 4).

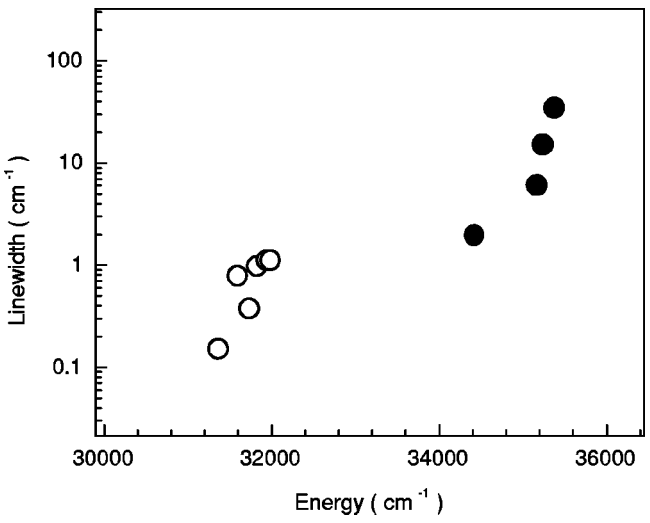

FIG. 12. Average widths of TPE lines observed in each of the $^8S_{7/2}\rightarrow{}^6I_J$ and ^6D_J transitions for cubic-site Eu^{2+} plotted against the energy of the ^6I_J (open circle) and ^6D_J (closed circle) levels. Similar results were obtained for non-cubic-site Eu^{2+}.

increase as the energy of the manifold increases. This indicates that mixing of the $4f^7$ levels with the $5d$ state becomes stronger for higher-lying $4f^7$ levels. A similar result has been reported for the linewidths of $4f^7$ levels of Eu^{2+} in SrF_2 and CaF_2 by Downer *et al.*[13] They suggested that the higher $4f^7$ levels vibrationally couple more strongly to neighboring sextet levels of $4f^65d$ than the lower levels to neighboring octets.

It is observed that cubic-site Eu^{2+} in $KMgF_3$ has much narrower and better-resolved TPE lines in each of the ^6I_J manifolds than cubic-site Eu^{2+} in CaF_2 and SrF_2, and moreover the TPE lines belonging to one manifold are separated from the TPE lines belonging to other ^6I_J manifolds. As a result, unlike the cases of alkaline-earth fluorides, there is no difficulty in identifying the observed lines in each of the ^6I_J manifolds in $KMgF_3$.

A different TPE spectrum was obtained in the range of the $^8S_{7/2}\rightarrow{}^6D_{9/2}$ transition by Francini *et al.*[6] than by us (see Sec. III): Francini *et al.* observed that the TPE line at 34 385 cm^{-1} (i.e., the *A* line in Fig. 2) is rather smaller in intensity than the line at 34 399 cm^{-1} (*B* line), while we observe the two lines with almost the same intensity. The *A* line is due to non-cubic-site Eu^{2+} because it is observed in the TPE spectrum for the $^6P_{7/2}$ emission but not observed in the TPE spectrum for the $^6I_{7/2}$ emission. Another difference was ob-

served between the OPE and TPE spectra in the $^8S_{7/2} \rightarrow {}^6I_{7/2}$ transition region as mentioned in Sec. III: some lines, observed in the OPE spectrum by Ellens *et al.*[5] are not observed in our TPE spectrum. The different results are observed when the excitation spectrum is measured by monitoring the $^6P_{7/2}$ emission. Observation of the $^6P_{7/2}$ emission gives information on the non-cubic-site Eu^{2+} ions as mentioned above. There are several kinds of non-cubic-site Eu^{2+} ions with symmetries of C_{4v}, C_{3v}, etc., depending on the location of the charge-compensating vacancy.[3] The ratio of populations among these ions with different site symmetries is expected to be different among different samples, resulting in the different experimental results of Francini *et al.* and Ellens *et al.* compared to ours.

V. CONCLUSION

Two-photon excitation spectroscopy was used to investigate the $4f^7$ levels of Eu^{2+} in $KMgF_3$, which are overlapped by the parity-allowed $4f^6 5d$ absorption band and thus not observable by one-photon excitation spectroscopy. The TPE spectrum of the $^6I_{7/2}$ emission is observed to be different from that of the $^6P_{7/2}$ emission. This is ascribed to the location of the $4f^6 5d$ state below the $^6I_{7/2}$ level for non-cubic-site Eu^{2+}; as a result the $^6I_{7/2}$ emission is produced by only cubic-site Eu^{2+}, while the $^6P_{7/2}$ emission is produced by not only cubic-site Eu^{2+} but also non-cubic-site Eu^{2+}. The observed TPE spectra give information on the position of the ^6I_J $(J=\frac{7}{2},\frac{9}{2},\frac{17}{2},\frac{11}{2},\frac{15}{2},\frac{13}{2})$ and ^6D_J $(J=\frac{9}{2},\frac{1}{2},\frac{7}{2},\frac{3}{2},\frac{5}{2})$ levels for both cubic- and non-cubic-site Eu^{2+}.

ACKNOWLEDGMENT

This work was supported by the BSRI Program (Grant No. BSRI-98-2411), Ministry of Education, Republic of Korea.

*Corresponding author: Email address: hjseo@dolphin.pknu.ac.kr

[1] O.J. Rubio, J. Phys. Chem. Solids **52**, 101 (1991).
[2] G. Blasse and B.C. Grabmaier, *Luminescent Materials* (Springer, Heidelberg, 1994), Chap. 3.3.
[3] T. Tsuboi and A. Scacco, J. Phys.: Condens. Matter **10**, 7259 (1998).
[4] N.S. Altshuler, L.D. Livanova, and A.L. Stolov, Opt. Spectrosc. **36**, 72 (1974).
[5] A. Ellens, A. Meijerink, and G. Blasse, J. Lumin. **59**, 293 (1994).
[6] R. Francini, U.M. Grassano, M. Tomini, S. Boiko, G.G. Tarasov, and A. Scacco, Phys. Rev. B **55**, 7579 (1997).
[7] R. Francini, U.M. Grassano, S. Boiko, G.G. Tarasov, and A. Scacco, J. Chem. Phys. **110**, 457 (1999).
[8] R.L. Schwiesow and H.M. Crosswhite, J. Opt. Soc. Am. **59**, 592 (1969).
[9] R.L. Schwiesow and H.M. Crosswhite, J. Opt. Soc. Am. **59**, 602 (1969).
[10] A.H. Piksis, G.H. Dieke, and H.M. Crosswhite, J. Chem. Phys. **47**, 5083 (1967).
[11] J.S. Detrio, M.W. Ferralli, and P.P. Yaney, J. Chem. Phys. **53**, 4372 (1970).
[12] G.H. Dieke, *Spectra and Energy Levels of Rare Earth Ions in Crystals* (Interscience Publishers, New York, 1968), pp. 250–252.
[13] M.C. Downer and C.D. Cordero-Montalvo, Phys. Rev. B **28**, 4931 (1983).
[14] M. Casalboni, R. Francini, U.M. Grassano, and R. Pizzoferrato, Cryst. Lattice Defects Amorphous Mater. **16**, 261 (1987).
[15] R.D. Shannon, Acta Crystallogr., Sect. A: Cryst. Phys., Diffr., Theor. Gen. Crystallogr. **32**, 751 (1976).
[16] J. Sytsma, G.F. Imbusch, and G. Blasse, J. Chem. Phys. **91**, 1456 (1989).
[17] M. Bouazaoui, B. Jacquier, C. Linares, and W. Strek, J. Phys.: Condens. Matter **3**, 921 (1991).
[18] L. Kundu, A.K. Banerjee, and M. Chowdhury, Chem. Phys. Lett. **181**, 569 (1991).
[19] W.T. Carnall, P.R. Fields, and K. Rajnak, J. Chem. Phys. **49**, 4443 (1968).